Directional and non-directional representations for the characterization of neuronal morphology

Burcin Ozcan[a], Demetrio Labate[a], David Jiménez[b], Manos Papadakis[a]

[a] Department of Mathematics, University of Houston
[b] Department of Mathematics, University of Costa Rica

ABSTRACT

The automated reconstruction of neuronal morphology is a fundamental task for investigating several problems associated with the nervous system. Revealing the mechanisms of synaptic plasticity, signal transmission, network connectivity and circuit dynamics requires accurate quantitative analyses of digital three-dimensional reconstructions. Yet, while many commercial and non-commercial software packages for neuronal reconstruction are available, these packages typically provide limited quantitative information and require a significant manual intervention. Recent advances in applied harmonic analysis, especially in the area of multiscale representations, offer a variery of techniques and ideas which have the potential to dramatically impact this very active field of scientific investigation. In this paper, we apply such ideas for (i) the derivation of a multiscale directional representation from isotropic filters aimed at detecting tubular structures and (ii) the development of a multiscale quantitative measure capable of distingushing isotropic from anisotropic structures. We showcase the application of these methods for the extraction of geometric features used for the detection of somas and dendritic branches of neurons.

1. INTRODUCTION

The automated morphological reconstruction of neurons imaged by optical or fluorescent microscopy is a challenging problem for which many algorithms and software packages have been proposed over many years.[6] However, even the most sophisticated of such packages have serious limitations, due to the difficulty of processing accurately complex three-dimensional data sets which are affected by many sources of noise and signal degradation. The main task of a typical algorithm for the automated reconstruction of neuronal morphology consists of segmenting the somas and the axonal and dendritic branches of neurons in a way which is suitable for quantitative analysis and computational modeling. A variety of methods have been employed to carry out this task. The purpose of this paper is to illustrate the application of some powerful and innovative methods emerged in the area of multiscale representations during the last decade and whose impact in the applied science has not been fully exploited yet. Such methods include *directional* multiscale representations such as curvelets,[2] shearlets[10] and wavelets with composite dilations,[5] which are designed to encode data containing anisotropic features with higher efficiency than traditional multiscale systems; they also include isotropic wavelets[11, 12] which provide special rotation covariance properties. Thanks to their ability to capture the geometry of high-dimensional data with high efficiency, this new generation of multiscale methods can be especially useful for the extraction of the intrinsic geometric features of neurons. In particular, we will illustrate two specific applications of this ideas to (i) the detection of tubular structures and (ii) the characterization of local isotropy.

The detection of tubular structure, in particular, is motivated by the to task of segmenting the axonal and dendritic branches of neurons. To facilitate this problem, we introduce a novel directional representation derived from isotropic filters which acts as a two dimensional Laplacian at the direction of the gradient of the intensity level of the image. This representation is applicable to images which contain tubular structures along with more isotropic ones. A similar ideas was used by one of the authors in a face recognition application to identify face components[4] such as eyes, nose and mouth. In this case, the singularity curves are used to model the edge boundaries associated with those face components. Since our representation acts locally, it is able to pick derivatives at the direction of the image intensity gradient which is the direction of the singularity curves.

Note that our new directional representation (Theorem 2.2, item 3, below) differs from other directional representations appeared in the literature such as shearlets and curvelets since it does not have predetermined directional subbands. In

E-mail: BO: bozcan@math.uh.edu, DL: dlabate@math.uh.edu, DJ: djimenez81@gmail.com, MP: mpapadak@math.uh.edu

reality, this representation is implemented by isotropic filters which act as directional filters by automatically aligning perpendicularly to the direction of the singularity curves. As a result, this representation does not exhibit the sparsity properties of shearlets and curvelets but it is computationally less intensive which is a significant advantage to deal with large-size data. On the other hand, numerical experiments have shown the benefits of a combined application of the proposed directional representation together with the shearlet representation, especially when the boundaries of the tubular structure are faint or blurred.

The second problem considered in this paper is the development of an automated method to distinguish tubular from non-tubular structures, and is motivated by the need to automatically identify the somas in images containing several neurons. We introduce a new concept of multiscale local isotropy which is inspired by the theory of directional multiscale representations (e.g., shearlets) and which allows us to define a quantitative measure of local isotropy. Our numerical experiment show that the application of this method is very competitive in segmenting somas, even in the situation of confocal images of cultured neurons where there are several colluded somas and their intensities are far from being uniform.

2. DIRECTIONAL REPRESENTATIONS FROM OMNIDIRECTIONAL CYLINDRICAL SINGULARITY DETECTORS IN 3D FROM ISOTROPIC FILTERS

We begin by introducing a generic model for tubular structures such as dendrites and axons. Clearly, a similar model is also applicable to other tubular structures such as blood vessels and branches of the bronchial tree.

2.1. Modeling tubular structures

We denote by $\mathbf{e}_1 = (1,0,0)$, $\mathbf{e}_2 = (0,1,0)$ and $\mathbf{e}_3 = (0,0,1)$. A plain cylinder in $\mathbb{R}^3$ can be modelled using the tensor product of a compactly supported function $g_{l_1,l_2}(x)$ and of a Gaussian $g_r(y,z) = e^{-(y^2+z^2)/r^2}$:

$$f_{l_1,l_2,r}(x,y,z) = g_{l_1,l_2}(x) g_r(y,z) \;\; x,y,z, \in \mathbb{R} \; r > 0.$$

The first of the two is even, non-increasing on the positive half axis and satisfies

$$\begin{array}{lll} g_{l_1,l_2}(x) = 1 & \text{if} & 0 \le x \le l_1 \\ g_{l_1,l_2}(x) > 0 & \text{if} & l_1 < x < l_2 \\ g_{l_1,l_2}(x) = 0 & \text{if} & l_2 \le x. \end{array}$$

Assumptions: Factor g_{l_1,l_2} controls the length of this generic tube, while the second factor controls the decay of the image intensity values in a cross-section of this structure. We assume that g_{l_1,l_2} and its first-order derivative are both absolutely continuous, so g'_{l_1,l_2} and g''_{l_1,l_2} are both absolutely integrable. In the prototype model the x-axis is the centerline of $f_{l_1,l_2,r}$.

Needless to mention that a generic tube in 2D has a similar structure and our analysis below applies verbatim to 2D as well. Henceforth, we fix the dimension of the underlying Euclidean domain to three. Any prototype cylinder can be reoriented by applying a 3D rotation R on the argument of $f_{l_1,l_2,r}$ so that its centerline points to the desired direction. In this paper, we assume that acquisition is isotropic and the bandwidth is sufficiently large to not generate aliasing artifacts due to the spatial orientation of the cylinder. The former assumption is used to simplify of our arguments. In practice, anisotropic sampling grids are used to reduce quantum light artifacts such as photo bleaching. The action, in this more general case, of the isotropic Laplacian filters h and ϕ defined below is studied in.[8] Now, let R be a 3D rotation matrix, that is, take $R \in SO(3)$, and denote $\mathscr{R}f(x,y,z) := f(R(x,y,z))$. A dendritic arbor $\mathscr{I}$ of a neuron can then be modelled as finite sum of simple tubular structures, that is:

$$\mathscr{I} = \sum_{i=1}^{n} \sum_{k=1}^{K} \sum_{j=1}^{J} a_{i,k,j} \; T_{\mathbf{x}_i} \mathscr{R}_k f_{l_j,L_j,r_j}, \quad \mathscr{R}_k \in SO(3), \quad a_{i,k,j} > 0,$$

where $R_1, R_2, \ldots, R_K$ are the 3D rotations corresponding to $\mathscr{R}_1, \mathscr{R}_2, \ldots, \mathscr{R}_K$ and $T_{x_i} f(x) := f(x - x_i)$, $x \in \mathbb{R}^3$. Here, $a_{i,k,j} > 0$ is a constant representing the maximum image intensity along the centerline of the tubular segment $T_{x_i} \mathscr{R}_k f_{l_j,L_j,r_j}$. At this point we assume that the intensity along the centerline of any component $T_{\mathbf{x}_i} \mathscr{R}_k f_{l_j,L_j,r_j}$ of the tubular structure is constant. Specializing to dendrites and axons, this assumption is practically equivalent to accepting that the concentration of the fluorescent dye along a dendritic branch is constant. To make this assumption more realistic we point that our model also accounts for the case where tubular segments are taken short enough allowing thus, the fluorescent agent concentration to be considered as constant in each one of these short segments, but, overall, the concentration can vary within the dendritic arbor.

2.2. Detection of tubular structures

Now, let $\phi \in L^2(\mathbb{R}^3)$ be a radial function such that $\xi \mapsto ||\xi||^2\hat{\phi}(\xi)$ is also absolutely integrable and bounded. Now define h by $\hat{h}(\xi) := ||\xi||^2\hat{\phi}(\xi)$, $\xi \in \mathbb{R}^3$. In addition, we assume that ϕ and all of its derivatives up second order are absolutely integrable.

Before proceeding to the rest of this section, we need to introduce a local Cartesian coordinate system adopted for each contributing part $T_{\mathbf{x}_i}\mathscr{R}_k f_{l_j,L_j,r_j}$ of the tubular structure. The axes of this local Cartesian system are the original x,y,z axes of the $\mathbb{R}^3$ reoriented by the action of the rotation R_k and the origin $(0,0,0)$ is shifted to $\mathbf{x}_i$.

By changing variables and by using the radiality of h, we infer

$$(T_{\mathbf{x}_i}\mathscr{R}_k f_{l_1,l_2,r} * h)(\mathbf{x}) = \int_{\mathbb{R}^3} f_{l_1,l_2,r}\left(R_k(\mathbf{x}-\mathbf{x}_i)-s\right)h(R_k^T s)ds = f_{l_1,l_2,r} * h\left(R_k(\mathbf{x}-\mathbf{x}_i)\right) \ . \tag{1}$$

Apparently the same equality is also valid with ϕ instead of h:

$$(T_{\mathbf{x}_i}\mathscr{R}_k f_{l_1,l_2,r} * \phi)(\mathbf{x}) = f_{l_1,l_2,r} * \phi\left(R_k(\mathbf{x}-\mathbf{x}_i)\right). \tag{2}$$

The continuity of $f_{l_1,l_2,r}$ and the integrability of $\hat{h}$ imply

$$f_{l_1,l_2,r} * h\left(R_k(\mathbf{x}-\mathbf{x}_i)\right) = \int_{\mathbb{R}^3} \hat{f}_{l_1,l_2,r}(\xi)\hat{\phi}(\xi)||\xi||^2 e^{2\pi i\xi\cdot(R_k(\mathbf{x}-\mathbf{x}_i))}d\xi = \Delta(f_{l_1,l_2,r}*\phi)\left(R_k(\mathbf{x}-\mathbf{x}_i)\right) \ .$$

Therefore, we conclude

$$(T_{\mathbf{x}_i}\mathscr{R}_k f_{l_1,l_2,r} * h)(\mathbf{x}) = \Delta(f_{l_1,l_2,r}*\phi)\left(R_k(\mathbf{x}-\mathbf{x}_i)\right) = \frac{\partial^2}{\partial x^2}(f_{l_1,l_2,r}*\phi)(\mathbf{x_0}) + \left(\frac{\partial^2}{\partial y^2}+\frac{\partial^2}{\partial z^2}\right)(f_{l_1,l_2,r}*\phi)(\mathbf{x_0})\,, \tag{3}$$

where $\mathbf{x_0} = R_k(\mathbf{x}-\mathbf{x}_i)$. Eq. (3) is the key observation that leads to Theorem 1. That is, the 3D-isotropic Laplacian of the filtered output of the tubular structure has two components, the axial and the cross-sectional 2D Laplacian; the former is negligible but the latter practically equals the 3D Laplacian. This observation will help us to show that the action on the tubular structure of the 3D-isotropic Laplacian filters is essentially equivalent to the action of cylindrically symmetric directional 2D Laplacian filters filters. A similar statement holds true for ϕ as well. All these facts are articulated in Theorem 1.

Now, pick an accuracy threshold $\varepsilon > 0$. We make the simplifying assumption that $\mathbf{x_0}$ is sufficiently away from both ends of the tubular structure $f_{l_1,l_2,r}$. In fact, under this assumption we practically imply that the spatial extend of filter ϕ is relatively smaller than that of the tubular structure of the dendritic branch. More precisely, we assume $|\mathbf{x}_0\cdot\mathbf{e}_1| + r_0 < l_1$. Therefore, with no loss of generality we can shift the axial center of the tubular structure from the origin to another point on the x-axis so that $\mathbf{x_0} = (0, y_{0,1}, z_{0,1})$. Now, the integrability of $\xi \mapsto ||\xi||^2\hat{\phi}(\xi)$ and the well-known Riemann-Lebesgue lemma imply that we can select $r_0 > 0$ such that $|D^\alpha\phi(\mathbf{y})| < \min\{\varepsilon/2l_2, \varepsilon\}$, if $||\mathbf{y}|| \geq r_0$ and $|\alpha| \leq 2$. These two observations are summarized in the following lemma:

LEMMA 2.1. *Let $\varepsilon > 0$ and $\phi \in L^1(\mathbb{R}^3)$ be a radial function such that $\xi \mapsto ||\xi||^2\hat{\phi}(\xi)$ is also absolutely integrable and $D^\alpha\phi \in L^1(\mathbb{R}^3)$ for all $|\alpha| \leq 2$. Then, there exists $0 < r_0$ such that:*

1. $|D^\alpha\phi(\mathbf{y})| < \min\{\varepsilon/2l_2, \varepsilon\}$ *if* $||\mathbf{y}|| \geq r_0$ *and* $|\alpha| \leq 2$.
2. $\int_{|x|>r_0} |D^\alpha\phi| < \varepsilon$.

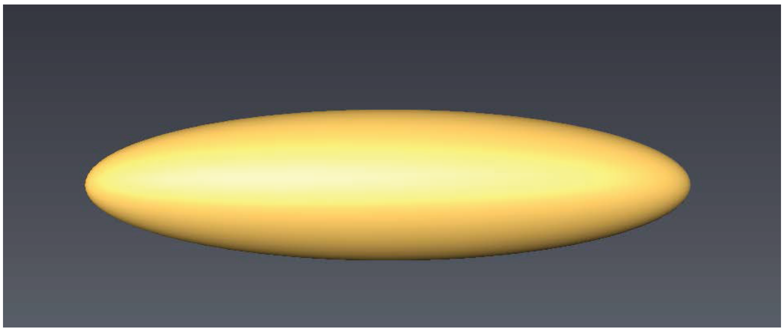

Figure 1. Volume rendering of the directional filter ω derived from ϕ which automatically aligns itself locally with the axis of the tubular structure

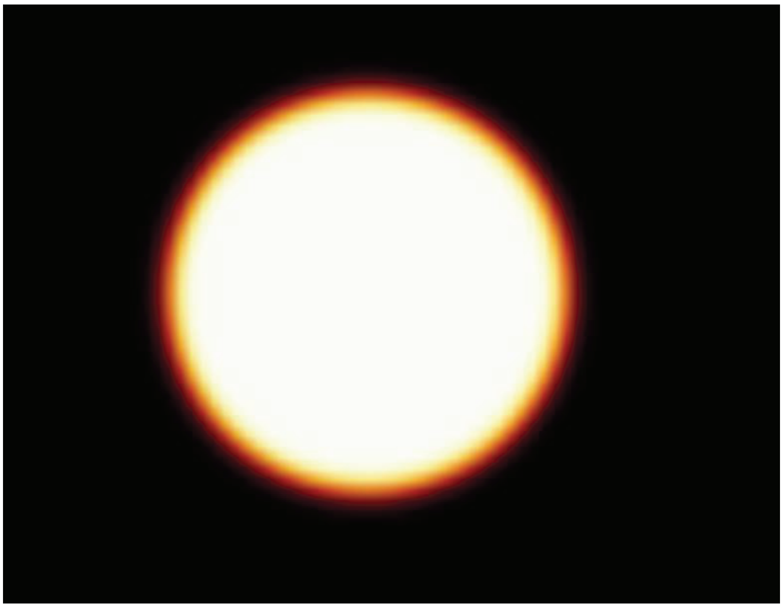

Figure 2. The cross section at the center of its symmetry of ω shown in Fig. 1. This cross section is equal to a specific example of ω.

In other words, we choose filters ϕ with a sufficient smoothness and spatial localization. One way to achieve this is to choose $r_0 < l_1/4$. In practice, we don't work with a single filter ϕ but with an ensemble of filters living at different scales, from fine to coarse provided that we maintain the requirement $|\mathbf{x}_0 \cdot \mathbf{e}_1| + r_0 < l_1$. These mathematical considerations reaffirm what we have seen in practice: Filters with bigger r_0 are be suitable for thicker and longer tubular structures while the ones with a smaller r_0 are fit to capture short and thin tubular structures.

THEOREM 2.2. *Let $\varepsilon > 0$ and $\phi \in L^1(\mathbb{R}^3)$ be a radial function such that $\xi \mapsto \|\xi\|^2 \hat{\phi}(\xi)$ is also absolutely integrable and $D^\alpha \phi \in L^1(\mathbb{R}^3)$ for all $|\alpha| \leq 2$ and $r_0 > 0$ be as in Lemma 2.1. Then, the following are true:*

1. *For every point $\mathbf{x}$ that is sufficiently far from the endpoints of the tubular structure $T_{\mathbf{x}_i}\mathscr{R}_k f_{l_1,l_2,r}$, in the sense $\left|(\mathbf{x}-\mathbf{x}_i)\cdot(R_k^T \mathbf{e}_1)\right| + r_0 < l_1$, we have*
$$\left|(T_{\mathbf{x}_i}\mathscr{R}_k f_{l_1,l_2,r} * \phi)(\mathbf{x}) - g_r * \omega\left(y(\mathbf{x}_0), z(\mathbf{x}_0)\right)\right| \leq \|g_r\|_1 \varepsilon \,,$$
where $y(\mathbf{x}_0)$ and $z(\mathbf{x}_0)$ are the second and third components of $\mathbf{x}_0$ respectively and
$$\omega(y,z) := \int_{\mathbb{R}} \phi(x,y,z)dx \,. \tag{4}$$

2. *Filtering the tubular structure with the 3D Isotropic Laplacian filter h practically amounts to applying the 2D Laplacian on the cross-section of the tubular structure $T_{\mathbf{x}_i}\mathscr{R}_k f_{l_1,l_2,r}$: Specifically, for every $\mathbf{x}$ as in the previous item we have*
$$\left|(T_{\mathbf{x}_i}\mathscr{R}_k f_{l_1,l_2,r} * h)(\mathbf{x}) - g_r * \Delta_{y,z}\omega\left(y(\mathbf{x}_0), z(\mathbf{x}_0)\right)\right| < 3\|g_r\|_1 \varepsilon$$
where, $\Delta_{y,z} = \frac{\partial^2}{\partial y^2} + \frac{\partial^2}{\partial z^2}$. Hence, for all practical purposes, the outcome of the filtering process of the tubular structure with both ϕ and h depends only on the relative position of the point $\mathbf{x}$ with respect to the cross-section of the tubular structure derived by the plane containing $\mathbf{x}$ and by the properties of this cross-section.

3. *Moreover, the filtering with the 3D isotropic filters ϕ and h is equivalent to filtering with directional filters that automatically align themselves with the axis of the tubular structure. More precisely, if $0 < r_0 < r_1$, where $\left|(\mathbf{x}-\mathbf{x}_i)\cdot(R_k^T \mathbf{e}_1)\right| + r_1 < l_1$ and $C = \int_{\mathbb{R}} g_{r_0,r_1}(x)dx$, then the following are true:*
$$\left|(T_{\mathbf{x}_i}\mathscr{R}_k f_{l_1,l_2,r} * \phi)(\mathbf{x}) - \frac{1}{C} T_{\mathbf{x}_i}\mathscr{R}_k f_{l_1,l_2,r} * \mathscr{R}_k(\omega g_{r_0,r_1})(\mathbf{x})\right| \leq \|g_r\|_1 \varepsilon, \tag{5}$$
and
$$\left|(T_{\mathbf{x}_i}\mathscr{R}_k f_{l_1,l_2,r} * h)(\mathbf{x}) - \frac{1}{C} T_{\mathbf{x}_i}\mathscr{R}_k f_{l_1,l_2,r} * \mathscr{R}_k\left((\Delta_{y,z}\omega) g_{r_0,r_1}\right)(\mathbf{x})\right| < 3\|g_r\|_1 \varepsilon \tag{6}$$

The proof of Theorem 2.2 is given in[8] and for more general cross-sections g_r's.

Theorem 2.2 will next be used to derive a method to detect the boundary surface of the tubular structure. Since Gaussian functions are supported over the entire real line we must now incorporate in our model the location of the boundary of the tubular structure. This has not been done so far and to the best of our knowledge we are the first to propose this addition to the model. Taking into account
$$\Delta_{y,z} g_r(\rho) = \frac{1}{\rho}\frac{\partial}{\partial \rho}\left(\rho \frac{\partial\left(e^{-\frac{\rho^2}{r^2}}\right)}{\partial \rho}\right) = \frac{2e^{-\frac{\rho^2}{r^2}}}{r^2}\left(\frac{2\rho^2}{r^2} - 1\right) \quad \rho > 0 \,,$$
we postulate that the boundary of the tubular structure is located at radial distance $r/\sqrt{2}$ from the centerline. This radius coincides with the inflection point of the cross-section g_r. We choose to model the tubular structure boundary at this radius, since it is the rate of decay of the values g_r gradually slows down for radial distances greater than $r/\sqrt{2}$. This theoretical model naturally associates with the observed gradual decay of the fluorescent intensity expressed by counts of photons originating from the boundary region of the tubular structure. According to this theoretical model for the

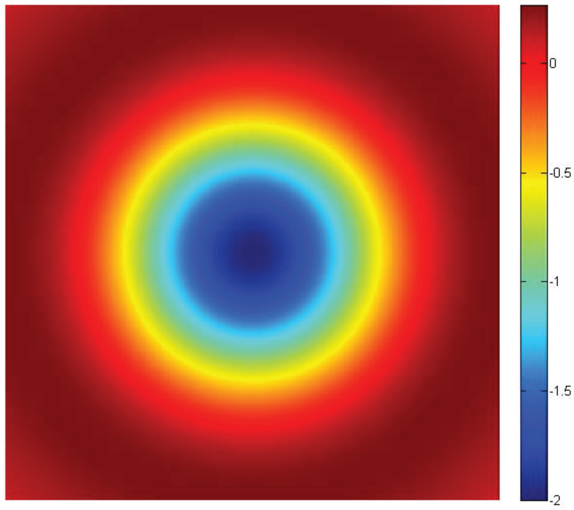

Figure 3. Color representation of the Laplacian where ϕ is a 2D Gaussian.

tubular structure, the change in the sign of the second order derivative of the Gaussian cross-section can characterize the boundary of the structure better than the values of the Gaussian function itself, especially, when the fluorescent dye has weak concentrations, e.g. in distal dendritic branches, and thus intensity values do not decay fast enough to allow a threshold-based discrimination of the structure from the background with sufficient confidence. This change in the sign of $\Delta_{y,z}g_r$ is what we use as one of the features in order to segment the volume of the dendritic arbor and of axons. This segmentation[9] also gives us the somas in the same volume with dendritic arbors. The next step is to find how filtering with ϕ can capture accurately the change in the sign of $\Delta_{y,z}g_r$.

PROPOSITION 2.3. *Assume that the hypotheses of Theorem 2.2 hold true and* $\left|1-\hat{\phi}(\xi)\right| < \varepsilon$ *for a.e.* $||\xi|| < r_0$. *Let also* $K > 0$ *be such that* r_0 *of Lemma 2.1 satisfies* $r_0 > \frac{K}{r}$ *where* K *is determined by*

$$\int_{||(\xi_2,\xi_3)||>\frac{K}{r}} \widehat{g_r}(\xi_2,\xi_3)(\xi_2^2+\xi_3^2)d\xi_2 d\xi_3 < \frac{\varepsilon}{1+||\phi||_1} . \tag{7}$$

Then, for every x_i *and rotation* R_k *we have*

$$\left|(T_{\mathbf{x}_i}\mathscr{R}_k f_{l_1,l_2,r} * h)(\mathbf{x}) - \Delta_{y,z}g_r\left(y(\mathbf{x}_0),z(\mathbf{x}_0)\right)\right| \le (3||g_r||_1+1)\varepsilon$$

for every $\mathbf{x}$ *that is sufficiently far from the endpoints of the tubular structure* $T_{\mathbf{x}_i}\mathscr{R}_k f_{l_1,l_2,r}$, *in the sense* $\left|(\mathbf{x}-\mathbf{x}_i)\cdot(R_k^T\mathbf{e}_1)\right| + r_0 < l_1$.

Proof: We begin by noting

$$\begin{aligned}
&\left|(T_{\mathbf{x}_i}\mathscr{R}_k f_{l_1,l_2,r} * h)(\mathbf{x}) - \Delta_{y,z}g_r\left(y(\mathbf{x}_0),z(\mathbf{x}_0)\right)\right| \\
&= \left|(T_{\mathbf{x}_i}\mathscr{R}_k f_{l_1,l_2,r} * h)(\mathbf{x}) - g_r * \Delta_{y,z}\omega\left(y(\mathbf{x}_0),z(\mathbf{x}_0)\right) - \Delta_{y,z}g_r\left(y(\mathbf{x}_0),z(\mathbf{x}_0)\right) + g_r * \Delta_{y,z}\omega\left(y(\mathbf{x}_0),z(\mathbf{x}_0)\right)\right| \\
&\le \left|(T_{\mathbf{x}_i}\mathscr{R}_k f_{l_1,l_2,r} * h)(\mathbf{x}) - g_r * \Delta_{y,z}\omega\left(y(\mathbf{x}_0),z(\mathbf{x}_0)\right)\right| + \left|g_r * \Delta_{y,z}\omega\left(y(\mathbf{x}_0),z(\mathbf{x}_0)\right) - \Delta_{y,z}g_r\left(y(\mathbf{x}_0),z(\mathbf{x}_0)\right)\right|;
\end{aligned}$$

From item 2 of Theorem2.2 we know that the first term of the previous sum does not exceed $3||g_r||_1\varepsilon$. Now, we need to show the second term is bounded above by 3ε. If we take the Fourier transform of second term, we get

$$(g_r * \Delta_{y,z}\omega - \Delta_{y,z}g_r)^\wedge(\xi_2,\xi_3) = \widehat{g_r}(\xi_2,\xi_3)(\xi_2^2+\xi_3^2)\widehat{\omega}(\xi_2,\xi_3) - \widehat{g_r}(\xi_2,\xi_3)(\xi_2^2+\xi_3^2) . \tag{8}$$

Now, we will show the norm of the right-hand side of Equation (8) is less than 3ε,

$$\int_{\mathbb{R}^2}\left|\widehat{g_r}(\xi_2,\xi_3)(\xi_2^2+\xi_3^2)\widehat{\omega}(\xi_2,\xi_3) - \widehat{g_r}(\xi_2,\xi_3)(\xi_2^2+\xi_3^2)\right|d\xi_2 d\xi_3 = \int_{\mathbb{R}^2}\widehat{g_r}(\xi_2,\xi_3)(\xi_2^2+\xi_3^2)|\widehat{\omega}(\xi_2,\xi_3)-1|d\xi_2 d\xi_3$$

$$\leq \int_{\|(\xi_2,\xi_3)\|\leq \frac{K}{r}} \widehat{g_r}(\xi_2,\xi_3)(\xi_2^2+\xi_3^2)|\widehat{\omega}(\xi_2,\xi_3)-1|d\xi_2 d\xi_3 + \int_{\|(\xi_2,\xi_3)\|\geq \frac{K}{r}} \widehat{g_r}(\xi_2,\xi_3)(\xi_2^2+\xi_3^2)(|\widehat{\omega}(\xi_2,\xi_3)|+1)d\xi_2 d\xi_3$$

Taking into account the assumptions $\left|1-\hat{\phi}(\xi)\right| < \varepsilon$ for a.e. $\|\xi\| < r_0$, (7) and the fact $\hat{\omega}(\xi_2,\xi_3) = \hat{\phi}(0,\xi_2,\xi_3)$ a.e. we conclude

$$\left|(T_{\mathbf{x}_i}\mathscr{R}_k f_{l_1,l_2,r} * h)(\mathbf{x}) - \Delta_{y,z} g_r\left(y(\mathbf{x}_0), z(\mathbf{x}_0)\right)\right| \leq (3\|g_r\|_1+1)\varepsilon \tag{9}$$

This completes the proof of Proposition 2.3.

An example of a filter ϕ satisfying the assumptions of Proposition 2.3 is given by

$$\hat{\phi}(\xi) = P_n\left(C_{n,\sigma}\|\xi\|^2\right) e^{-C_{n,\sigma}\|\xi\|^2},\ \xi \in \mathbb{R}^3$$

where P_n is the Taylor polynomial of degree n associated with the exponential function e^x and $C_{n,\sigma} = (n+1)/(2\pi\sigma)^2$. The functions ϕ of this type are called Hermite Distributed Approximating Functionals and were first proposed in.[7] Their main property is that their inflection point of $\hat{\phi}$ is at radial distance $2\pi\sigma$ from the origin. As it has been shown[1,3] the inflection point of $\hat{\phi}$ stays at this distance for every n. However, as n increases one can achieve $\hat{\phi}(\xi) \approx 1$ for a ball of radius $2\pi\sigma$. Specifically, for a given $\varepsilon > 0$ and $1 \leq b < 2$ we can determine n big enough so that $\left|1-\hat{\phi}(\xi)\right| < \varepsilon$ for a.e. $\|\xi\| < b\pi\sigma$.

To apply Proposition 2.3 we pick r_0 as prescribed by Proposition 2.3 and we need to take n big enough to secure

$$b\pi\sigma < r_0\ .$$

3. A MULTISCALE MEASURE OF LOCAL ISOTROPY

Let $A \subset \mathbb{R}^3$. If $x \in A$ we say that *A is locally isotropic at x and at scale $s > 0$ if $B(x,s/2) \subseteq A$.* Obviously the scale at which the isotropy is observed is not uniquely. For example, let A be a ball of radius $S > 0$. Then, the ball at its center is locally isotropic at any radius up to scale $2S$. However, as the point of interest moves closer to the boundary the scale of isotropy is being reduced, as expected. On the antipodal end let $f_{l_1,l_2,r}$ be a tubular structure as defined in the previous section. Then, at any point of its centerline the tubular structure has local isotropy of scale up to $2r$. So , at a small scale and in every structure with non-empty interior, an interior point can be regarded as a point of local isotropy. So, in order to distinguish structures which are highly directional such as a tube from other less directional structures, we propose to use the concept of local isotropy but the selection of the scale for this determination is critical. To accomplish this task we propose to use a family of very simple filters which are inspired by Radon transform:

Let, $0 < r < s$. Define

$$\chi_{s,r} := \chi_{[-\frac{s}{2},\frac{s}{2}]\times[-\frac{r}{2},\frac{r}{2}]^{(d-1)}}$$

and take the family of all of its rotations $\mathscr{R}\chi_{s,r}$. In practice, we consider only a finite set of rotations. The next result gives some rise to a quantity we call *Directional Ratio at scale s* (DR_s) defined by

$$DR_s(x) = \sup_{0<r<s} \frac{\min\{\langle \chi_A, T_x\mathscr{R}\chi_{s,r}\rangle : R \in SO(d)\}}{\max\{\langle \chi_A, T_x\mathscr{R}\chi_{s,r}\rangle : R \in SO(d)\}}\ ,$$

where $d = 2,3$ and x is an interior point of A (see Fig. 4). Note, that when x is an interior point of A the quantity $DR_s(x)$ is well defined for every scale $s > 0$. In any image, since even the finest structures have non-empty interior of width of at least one pixel/voxel, every point in the image is interior to some structure. So the function DR_s can be computed for every pixel/voxel.

PROPOSITION 3.1. *Suppose that A is a closed subset of $\mathbb{R}^3$ and that x is point of local isotropy of A at scale S. Then, $DR_s(x) = 1$ for every $0 < s \leq S$. Moreover, DR_s is locally rotationally invariant and scale and it also obeys a simple covariance rule under the action of rigid motions:*

For any rigid motion Q, the directional ratio of $Q(A)$ at Qx at any scale is equal to directional ratio of A at x at the same scale.

Last, DR_s obeys a simple scale covariance rule: For every closed subset A and scale s, the directional ratio for aA at ax, $DR_{as}(ax)$ is equal to the directional ratio for A at x $DR_s(x)$

Proof If x is point of local isotropy of A at scale S then the ball $B(x,S/2)$ is contained in A. Then, for a fixed $s \le S$ and any rotation R we have

$$\lim_{r\to 0} \left\langle \chi_{A\setminus B(x,\,S/2)},\, T_x\mathscr{R}\chi_{s,r} \right\rangle = 0 \,. \tag{10}$$

Moreover, the radial symmetry of $B(0,S/2)$ implies that for every $0<r<s$ we have $\left\langle \chi_{B(x,S/2)},\, T_x\mathscr{R}\chi_{s,r} \right\rangle = \left\langle \chi_{B(0,S/2)},\, \mathscr{R}\chi_{s,r} \right\rangle = \left\langle \chi_{B(0,S/2)},\, \chi_{s,r} \right\rangle$. The right-hand side of the previous equation depends only on r. Since, the representation $R \to \mathscr{R}$ is continuous on $SO(d)$ and the topology of pointwise convergence (Strong Operator Topology)in the space of bounded operators defined on $L^2(\mathbb{R}^d)$ and $SO(d)$ is compact there exist rotations $R_{1,r}$ and $R_{2,r}$ such that

$$\min\{\langle \chi_A, T_x\mathscr{R}\chi_{s,r}\rangle : R \in SO(d)\} = \langle \chi_A, T_x\mathscr{R}_{2,r}\chi_{s,r}\rangle$$

and

$$\max\{\langle \chi_A, T_x\mathscr{R}\chi_{s,r}\rangle : R \in SO(d)\} = \langle \chi_A, T_x\mathscr{R}_{1,r}\chi_{s,r}\rangle \,.$$

So,

$$\frac{\min\{\langle \chi_A, T_x\mathscr{R}\chi_{s,r}\rangle : R \in SO(d)\}}{\max\{\langle \chi_A, T_x\mathscr{R}\chi_{s,r}\rangle : R \in SO(d)\}} = \frac{\langle \chi_A, T_x\mathscr{R}_{2,r}\chi_{s,r}\rangle}{\langle \chi_A, T_x\mathscr{R}_{1,r}\chi_{s,r}\rangle} = \frac{\left\langle \chi_{B(0,S/2)},\, \chi_{s,r} \right\rangle + \left\langle \chi_{A\setminus B(x,\,S/2)},\, T_x\mathscr{R}_{2,r}\chi_{s,r} \right\rangle}{\left\langle \chi_{B(0,S/2)},\, \chi_{s,r} \right\rangle + \left\langle \chi_{A\setminus B(x,\,S/2)},\, T_x\mathscr{R}_{1,r}\chi_{s,r} \right\rangle}$$

which due to Eq. (10) implies

$$\lim_{r\to 0} \frac{\min\{\langle \chi_A, T_x\mathscr{R}\chi_{s,r}\rangle : R \in SO(d)\}}{\max\{\langle \chi_A, T_x\mathscr{R}\chi_{s,r}\rangle : R \in SO(d)\}} = 1 \,.$$

Now, we turn our attention to proof of the second statement of Proposition 3.1. By local rotational invariance we mean invariance to a rotation centered at x. Such a rotation is the composition of, first, of a shift by $-x$ moving the origin to x, then of a rotation and finally of a shift by x. Thus, the action of a local rotation centered at x on A is expressed by the action of the corresponding operators on χ_A. Therefore, the characteristic function of the set A transformed under the action of the local rotation centered at x is equal to $T_x\mathscr{Q}T_{-x}\chi_A$, where Q is the rotation matrix inducing $\mathscr{Q}$. Thus, for all s,r we have

$$\langle T_x\mathscr{Q}T_{-x}\chi_A, T_x\mathscr{R}\chi_{s,r}\rangle = \langle T_{-x}\chi_A, \mathscr{Q}^*\mathscr{R}\chi_{s,r}\rangle = \langle \chi_A,\, T_x(\mathscr{Q}^*\mathscr{R})\chi_{s,r}\rangle \,.$$

Since, $Q^T(SO(d)) = SO(d)$, we infer that $DR_s(x)$ of A and of A transformed under the action of the local rotation are equal. In a similar, fashion we derive the rotational covariance rule: For any $Q \in SO(d)$, the directional ratio of $Q(A)$ at Qx at any scale is equal to directional ratio of A at x at the same scale. The rule follows easily after observing $\mathscr{Q}T_{Qx} = T_x\mathscr{Q}$ and

$$\langle \mathscr{Q}^*\chi_A, T_{Qx}\mathscr{R}\chi_{s,r}\rangle = \langle \chi_A, T_x(\mathscr{Q}\mathscr{R})\chi_{s,r}\rangle \,,$$

for all $s,r>0$. The covariance rule for shifts is derived by adopting the previous steps for rotations. Finally, to prove scale covariance first take $a>0$, a scaling factor. Define a dilation operator $D_af(y) = f(\frac{y}{a})$, $y \in \mathbb{R}^d$. Observe, $D_a^*T_{ax} = T_xD_a^*$. Next, for $r<s$

$$\langle \chi_{aA}, T_{ax}\mathscr{R}\chi_{as,ar}\rangle = \langle D_a\chi_A, T_{ax}\mathscr{R}\chi_{as,ar}\rangle = \langle \chi_A, T_x\mathscr{R}D_a^*\chi_{as,ar}\rangle = \langle \chi_A, T_x\mathscr{R}\chi_{s,r}\rangle \,.$$

The previous equations imply that for every scale s, the directional ratio for aA at ax, $DR_{as}(ax)$ is equal to the directional ratio for A at x $DR_s(x)$ for every A. This completes the proof Proposition 3.1.

Next, we discuss if the converse statement of Proposition 3.1 is true. In particular, let us assume that if x is an interior point of A the measure of $B(x,S/2)\cap A^c$ is non-zero. If A is the ball $B(x,S/4)$ obviously $\lambda(B(x,S/2)\cap A^c) > 0$, but still, due to the rotational invariance of $B(x,S/4)$ the directional ratio at x and at scale S is still equal to 1, but x is not a point of isotropy for $B(x,S/4)$ at this scale. This example suggests that directional ratio alone is not sufficient to characterize points of isotropy of closed sets in 2D or 3D. However, with a bit of additional information it is feasible to obtain a partial converse of the first assertion of Proposition 3.1.

PROPOSITION 3.2. *Assume that A is a closed set with non-empty interior and x is an interior point of A. Moreover, assume that there exists $S>0$ and a rotation R such that $x + R^T([-\frac{s}{2},\frac{s}{2}] \times [-\frac{r}{2},\frac{r}{2}]^{(d-1)}) \subseteq A$ for some $0<r\le S$. If $DR_S(x) = 1$, then x is a point of isotropy of A at scale S.*

Proof: Let Q be an arbitrary rotation and $0 < p < r$, then we observe

$$\langle \chi_A, T_x \mathscr{Q} \chi_{S,p} \rangle = \|\chi_{A \cap (x + Q^T([-\frac{S}{2}, \frac{S}{2}] \times [-\frac{p}{2}, \frac{p}{2}]^{(d-1)}))}\| \leq S p^{d-1} \tag{11}$$

Hence,

$$\min\{\langle \chi_A, T_x \mathscr{Q} \chi_{S,p} \rangle : Q \in SO(d)\} \leq S p^{d-1}$$

for all $Q \in SO(d)$ and $p > 0$. On the other hand, the assumption $x + R^T([-\frac{S}{2}, \frac{S}{2}] \times [-\frac{r}{2}, \frac{r}{2}]^{(d-1)}) \subseteq A$ for some $0 < r \leq S$ and some rotation R implies, due to (11),

$$\max\{\langle \chi_A, T_x \mathscr{Q} \chi_{S,p} \rangle : Q \in SO(d)\} = S p^{d-1} .$$

To complete the proof we need to establish $B(x, S/2) \subseteq A$. Assume, that the contrary is true. Let $y \in B(x, S/2) \cap A^c$. Since A is closed, there exists $0 < p_0 < r$ such that $B(y, p_0) \subset B(x, S/2) \cap A^c$. Since $DR_S(x) = 1$, for any given $\varepsilon > 0$ and every $0 < p < p'$, where $p' < \min\{r, p_0/2\}$ and is determined by ε, we have

$$\frac{\min\{\langle \chi_A, T_x \mathscr{Q} \chi_{S,p} \rangle : Q \in SO(d)\}}{\max\{\langle \chi_A, T_x \mathscr{Q} \chi_{S,p} \rangle : Q \in SO(d)\}} \geq 1 - \varepsilon .$$

The previous inequality is also valid for an orientation $Q_0 \in SO(d)$ which moves the axis of the slab $x + R^T([-\frac{S}{2}, \frac{S}{2}] \times [-\frac{r}{2}, \frac{r}{2}]^{(d-1)})$ to the line segment connecting x and y. Then, inside the ball $B(y, p_0)$ we can find a smaller slab

$$y + Q_0^T \left(\left[-\frac{p_0}{2}, \frac{p_0}{2}\right] \times \left[-\frac{p}{2}, \frac{p}{2}\right]^{(d-1)} \right) .$$

This slab resides inside the bigger slab $x + Q_0^T([-\frac{S}{2}, \frac{S}{2}] \times [-\frac{p}{2}, \frac{p}{2}]^{(d-1)})$. However, the smaller slab is not contained in A but it is contained in A^c. Therefore,

$$\frac{S p^{d-1} - p_0 p^{d-1}}{S p^{d-1}} \geq \frac{\langle \chi_A, T_x \mathscr{Q} \chi_{S,p} \rangle}{S p^{d-1}} = \frac{\min\{\langle \chi_A, T_x \mathscr{Q} \chi_{S,p} \rangle : Q \in SO(d)\}}{\max\{\langle \chi_A, T_x \mathscr{Q} \chi_{S,p} \rangle : Q \in SO(d)\}} \geq 1 - \varepsilon .$$

Consequently, if we select $\varepsilon < p_0/S$, then we arrive at a contradiction. This argument completes the proof of this proposition.

Directional ratios at various scales are used for the segmentation of somas in fluorescent images of cultured neurons. After segmenting the volume of neuronal cells from the background will have a binary image were somas, dendrites and even axons are present. Axons and dendritic arbors have tubular structure therefore there directional ratio is small. On the other hand, somas are more isotopic therefore in their interior the directional ratio for relatively big scales S is high, as anticipated due to Proposition 3.1. The difference between the values of the directional ratio inside somas and in the more tubular parts of the images we analyze at the same scale S allows us to distinguish somas from dendrites. To identify the boundaries of somas are we use a level set approach where, in principle, evolutions are initialized is given by the boundary of the set $DR_S^{-1}(\{1\})$. The vector field for these evolutions is given by the gradient of DR_S. Typically, we use multiple scales S to drive these evolutions.

4. ACKNOWLEDGMENT

This work was partially supported by NSD-DMS 1320910, 0915242, 1008900, 1005799 and by NHARP-003652-0136-2009. We also want to thank Professor I.A. Kakadiaris for numerous helpful discussions on various topics in computer vision.

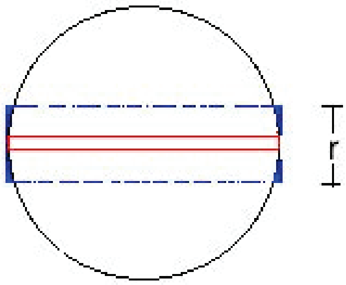

Figure 4. Illustration of the main idea of the definition of the function DR_s and of the proof of Proposition 3.1. As $r \to 0$ the parallilepiped $[-\frac{s}{2}, \frac{s}{2}] \times [-\frac{r}{2}, \frac{r}{2}]^{(d-1)}$ is almost contained in $B(x, s/2)$ if x is a point of isotropy of A at scale s, forcing $DR_s(x) = 1$.

REFERENCES

1. B.G. Bodmann, D.K. Hoffman, D.J. Kouri, and M. Papadakis. Hermite distributed approximating functionals as almost-ideal low-pass filters. *Sampling Theory in Image and Signal Processing*, 7:15–38, 2007.
2. A. Candes and D. Donoho. Curvelets a surprisingly effective nonadaptive representation for objects with edges. In L. Schumaker, editor, *Curves and Surfaces*, pages 105–120. Vanderbilt University Press, Nashville, TN, 2000.
3. C. Chandler and A. G. Gibson. Uniform approximation of functions with discrete approximation functionals. *J. Approx. Th.*, 100:233–250, 1999.
4. B. Efraty, M. Papadakis, A. Profitt, S. K. Shah, and I. A. Kakadiaris. Facial component landmark detection. In *Proc. 9^{th} IEEE International Conference on Automatic Face and Gesture Recognition*, pages 278 – 285, Santa Barbara, CA, Mar. 21-25 2011.
5. K. Guo, D. Labate, W. Lim, G. Weiss, and E. Wilson. Wavelets with composite dilations and their mra properties. *Appl. Comput. Harm. Anal.*, 20(2):202–236, March 2006.
6. M. Halavi, Kelly A. Hamilton, R. Parekh, and G. Ascoli. Digital reconstructions of neuronal morphology: Three decades of research trends. *Frontiers in Neuroscience*, 6(49), 2012.
7. D. K. Hoffman, N. Nayar, O. A. Sharafeddin, and D. J. Kouri. Analytic banded approximation for the discretized free propagator. *J. Phys. Chem.*, 95:8299–8305, 1991.
8. D. Jimenez, D. Labate, and M. Papadakis. Omnidirectionial representations from isotropic filters. Work in progress, 2013.
9. D. Jimenez, M. Papadakis, D. Labate, and I.A. Kakadiaris. Improved automatic centerline tracing for dendritic structures. In *Proc. International Symposium on Biomedical Imaging: From Nano to Macro*, San Francisco, CA, April 8-11 2013.
10. D. Labate, W.-Q. Lim, G. Kutyniok, and G. Weiss. Sparse multidimensional representation using shearlets. In M. Papadakis, A. F. Laine, and M. A. Unser, editors, *SPIE Conference Series*, volume 5914, pages 254–262, August 2005.
11. M. Papadakis, G. Gogoshin, I. A. Kakadiaris, D. J. Kouri, and D. K. Hoffman. Nonseparable radial frame multiresolution analysis in multidimensions and isotropic fast wavelet algorithms. In M. A. Unser, A. Aldroubi, and A. F. Laine, editors, *SPIE Conference Series*, volume 5207, pages 631–642, November 2003.

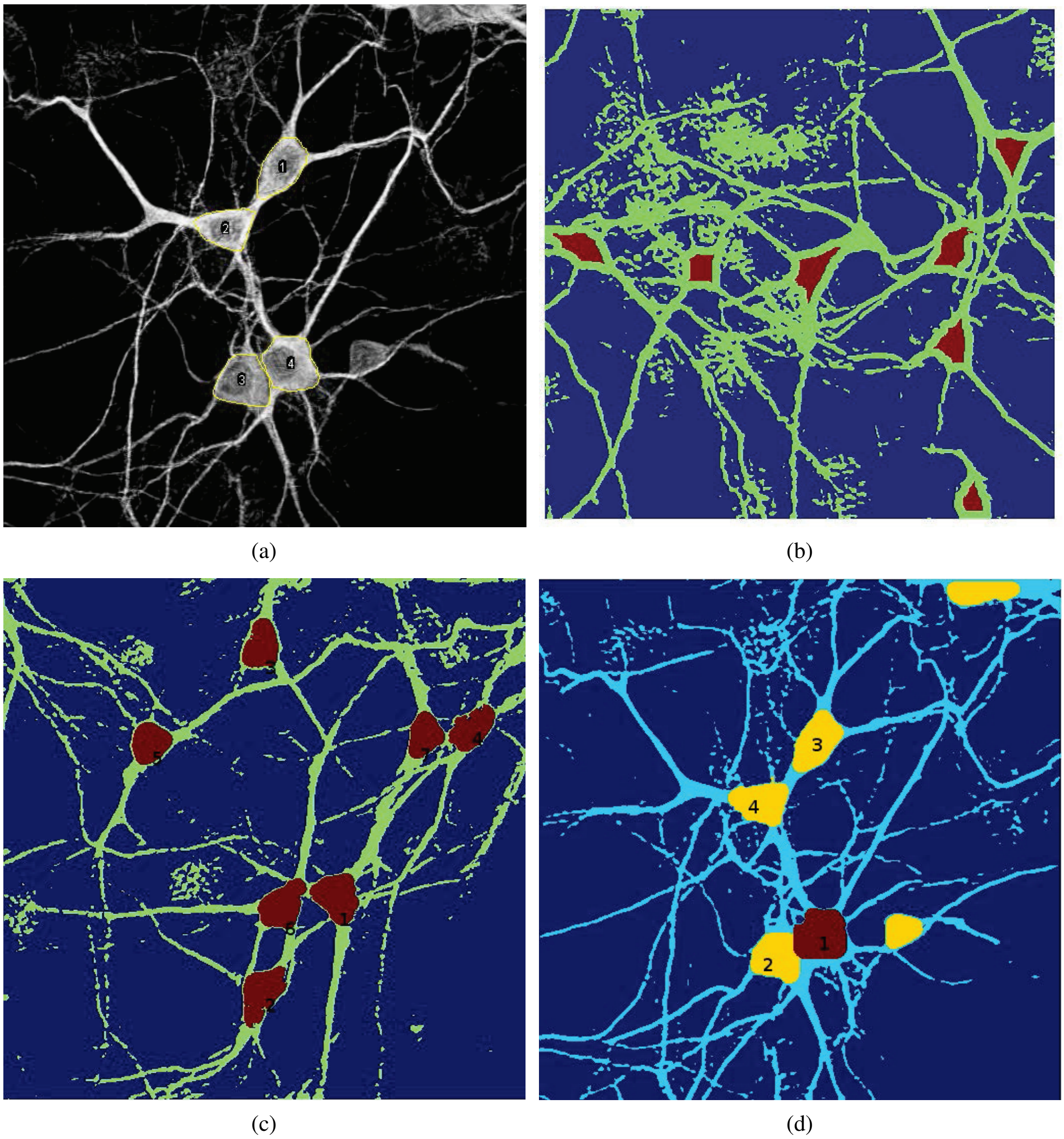

Figure 5. (a) Original image of cultured neurons. (b) Green indicates the segmented volume from the from the background indicated by blue. Somas can be distinguished in this image from the from the presence of red regions inside them. Those regions are $DR_S^{-1}(\{1\})$. The boundaries of these regions are used for the initialization of the level set evolutions. (c) Here the red regions indicate the segmented somas. (d) Red and yellow regions are the segmented somas in original (a). Using two separate evolutions we distinguish the two colluded somas numbered 1 and 2.

12. J.R. Romero, S.K. Alexander, S. Baid, S. Jain, and M. Papadakis. The geometry and the analytic properties of Isotropic Multiresolution Analysis. *Advances in Computational Mathematics*, 31:283–328, Oct. 2009.